TOPOLOGICAL REMESHING AND LOCALLY SUPPORTED SMOOTHING FOR BUBBLE COALESCENCE IN TWO-PHASE FLOWS

Gustavo Charles P. de Oliveira, tavolesliv@gmail.com
Norberto Mangiavacchi, norberto@uerj.br
State University of Rio de Janeiro, Faculty of Engineering, Rio de Janeiro, RJ, Brazil, 20940-903

Gustavo Anjos, rabello@mit.edu
Massachusetts Institute of Technology, Department of Nuclear Science and Engineering, Cambridge, USA, MA 02139

John R. Thome, john.thome@epfl.ch
École Polytechnique Fédéral de Lausanne, LTCM - Laboratoire de Transfert de Chaleur et de Masse, Station 9, Lausanne, Switzerland, CH-1015

Abstract. A dual strategy of remeshing and smoothing operations is introduced into the recent Arbitrary Lagrangian-Eulerian/Finite Element code developed for modeling of two-phase flows and heat transfer. At the forefront, the approach is introduced not only to discretize the continuum filled by the liquid and vapor phases but also to represent their common interface by computational elements. While in synchrony, a Level-Set (LS) methodology has now been introduced to better model the coalescing regions. Therefore, this work presents a two-dimensional idealized model concerning the numerical modeling of the coalescence between two circular bubbles immersed in stagnant liquid. While the ALE/FE approach can guarantee suitable remeshing to recover the structure of the mesh after the thin liquid film disruption, the LS strategy locally determines the coalescing region by application of a function of compact support. The effect of the collapse is assuaged and any sharpnesses owing to local topological changes occurring in the contact region tend to be less protruding by smoothing. Two-dimensional numerical results show that this incipient methodology is a promising technique in regard to coalescence studies and is able to be extended, a posteriori, to three-dimensional cases. Developed mainly to deal with bubble interactions, these strategies aim to be embodied, in the future, into a two-phase flow context, especially to simulate the coalescence taking place in transitional regions of passage from bubbly-to-slug and slug-to-annular patterns.

Keywords: Bubble coalescence, ALE formulation, Level-Set, Finite Element, Two-Phase Flow.

1. INTRODUCTION

In view of the growing field of applications involving multiphase flows, numerical tools have been developed to provide physical insight into the complex dynamics ocurring at interfacial regions shared by different fluids in their different phases. Inserted into this wider scope, gas-liquid flows cover a considerable range. They are present in chemical plants, oil pipelines, microevaporators, heat exchangers, cooling systems, just to cite a few examples. Some important patterns of two-phase flows are distinguished when gas bubbles permeate a continuum region of liquid either in a dispersive and disordered way, such as *bubbly* flows, or as elongated bubbles separated by liquid slugs, such as *slug* flows. Depending on the flow, the bubbles' surfaces may undergo plentiful transformations concerning their topology while interacting with one another. Generally, coalescence phenomena are initiated from these settings and their numerical simulation is an important objective of MCFD (Multiphase Computational Fluid Dynamics).

Recent papers evince bubble coalescence as one of the most relevant issues in modeling the dynamics of two-phase flows. For instance, Consolini and Thome (2010) included the coalescence in their analysis of the thin evaporating film present in micro-channel slug flows by verifying how it may influence the heat transfer. Coalescence was included by Ekambara *et al.* (2012) in their numerical modeling of gas-liquid bubbly flows. Coulibaly *et al.* (2013) studied the bubble coalescence in subcooled nucleate pool boiling cases. On the other hand, efficient MCFD models to represent the coalescence are on the summit of discussions. This work aims to introduce a promising new approach to assuage severe topological changes caused by the coalescence between two bubbles based on a combination between an ALE (Arbitrary Lagrangian-Eulerian) moving mesh formulation coupled with the Finite Element method and a Level-Set strategy enriched with a function whose support determines the coalescing region. Henceforward, we will refer to these strategies by the acronyms ALE/FE and LS.

Some strands of moving mesh methods applied to two-phase flows were lately disseminated in the literature as ALE/FE by dos Anjos (2012), PFEM (Particle Finite Element) by Mier-Torrecilla *et al.* (2011), and MMIT (Moving-Mesh Interface Tracking) by Quan (2011), Quan *et al.* (2009), Quan and Schmidt (2007). In all of them, the interface is described

by computational elements (nodes, edges, faces) upon a body-fitted Lagrangian fashion. Consequently, the nodes, primarily, are advected with the own flow velocity, so that the condition of sharp interface (zero-thickness) is maintained. This capability proposes a powerful advantage to simulate coalescence since the bubbles' boundaries deform as material surfaces. In the vein of these Lagrangian-like methods, another approach including LS imprints was presented by Sousa and Mangiavacchi (2005) at which the values of the level-set function is stored in each mesh node being, therefore, exempted of further calculations to attain smoothness. This work is rooted in a similar basis as regards the LS methodology, but it handles geometrical operations to remedy the mass unbalance that might come to pass at the coalescence region instead having to perform calculations of smoothing functions. The method also has the advantage to capture topological complexities occurring in the liquid thin film region between the bubbles because an algorithm based on distance calculations is applied. Next, the coalescence region is numerically determined by a function that pervades the original level-set function to confine the elements closer to the interfaces within a tolerance domain in order to mimic the real physics. This forcibly narrowed region is referred the *combination zone*.

Although the ALE/FE can be used for discretization of both computational domain and interfaces, the LS strategy is appended as a tool to determine the combination zone where the coalescence should take place. Examples of LS methods coupled to FE are Groß *et al.* (2006), in the context of multiphase flows, and Li and Shoppie (2011), concerning the interface-fitted representation. Aside from these studies, a general overview about LS methods is conducted by Osher and Fedkiw (2001).

Apart from their physical constitution, bubbles (also drops) may be recognized mathematically as topological surfaces - see Bloch (1956). In real applications involving two-phase flows, their boundaries may assume varying shapes depending on the flow pattern at which they emerge. Owing to this topological richness, formal terminologies could be coined. Shape regimes of bubbles were previously presented by Clift *et al.* (1978) in two major classes: static (sessile, pendant and floating bubbles) and free-motion (spherical, ellipsoidal and "spherical-cap" bubbles). Notwithstanding, incremental terminology appeared in the current literature. Some examples are cited by Michaelides (2006), such as "spherical cap with closed wake", "oblate ellipsoidal disk", and "skirted with wavy unsteady skirt".

At this point, it is worth to remember a few adimensional numbers that are related to bubble dynamics. Some of them are used to determine the shape regimes aforementioned. For instance, when interfacial effects are not negligible in the flow, the Weber number, *We*, is used to quantify the ratio between inertia and surface tension forces, whereas the Eötvös number, *Eo*, is used to quantify the ratio between buoyancy and surface tension forces. Besides, the classical Reynolds and Froude numbers, *Re* and *Fr*, are used in two-phase correlations as well. Equation (1) groups the definition of these numbers.

$$We = \frac{\rho_0 L_0 U_0^2}{\sigma_0}, \qquad Eo = \frac{\rho_0 g_0 D_0^2}{\sigma_0}, \qquad Re = \frac{U_0 L_0}{\nu_0}, \qquad Fr = \frac{U_0}{\sqrt{g_0 L_0}}, \tag{1}$$

where all the variables described are measures of reference chosen accordingly to the problem to be tackled, namely, length (L_0), velocity (U_0), density (ρ_0), gravity (g_0), diameter (D_0), surface tension (σ_0), and kinematic viscosity (ν_0). Furthermore, Eq. (2) defines another adimensional used to characterize the shape of bubbles. The Morton number *Mo* can be obtained by combining powers of We, Fr, and Re:

$$Mo = \frac{We^3}{Fr Re^4} \tag{2}$$

Some two-phase flow patterns are characterized by bubble interactions and are being extensively studied. We can refer to Cheng *et al.* (2008) for a review of flow patterns and maps. Coalescence phenomena observed in these flows are motivating a growing research interest. Recently, bubble dynamics studies for mass transfer purposes, for instance, were conducted by Agrawal (2013). Regarding nucleate boiling and chemical process, we can cite Jingliang *et al.* (2012).

Other flow patterns showing profuse topological changes are also identified in nuclear reactor applications as depicted in Fig. 1, an abridged picture extracted from Shen *et al.* (2012) which shows gas-liquid structures appearing on upward flows in a narrow rectangular channel. In such flows, bubble coalescence is common to happen mainly amid regime transitions and this issue is addressed by Julia and Hibiki (2011).

In horizontal microchannel two-phase flows, regime transitions are also observed. Among them, bubble-to-slug is a particular regime we will look at here. Figures 2 and 3 show macro-to-microchannel transition curves obtained through experimental studies in two-phase flows performed by Ong and Thome (2011) for the artificial refrigerant fluids R236fa and R134a, respectively, where there is an explicit zone where the coalescing bubble pattern takes place. They declare that, in some cases, the bubbles violently coalesce and no clear interface between the two phases can be seen. It is also emphasized in Revellin *et al.* (2008) that collision of bubbles in microchannels may be one of the most important parameters influencing flow pattern transition. In turn, such topological changes are a difficult task when tackled through MCFD methods.

Motivated by profuse topological complexity observed experimentally in several gas-liquid two-phase flow patterns, one first seeks MCFD methods more and more effective to compensate the shortcomings produced by discretization processes. Mass conservation errors, which contribute for a bad representation of the physical problem, could be emphasized

Figure 1: Two-phase upward flow structures in a narrow rectangular channel. Adapted from Shen *et al.* (2012).
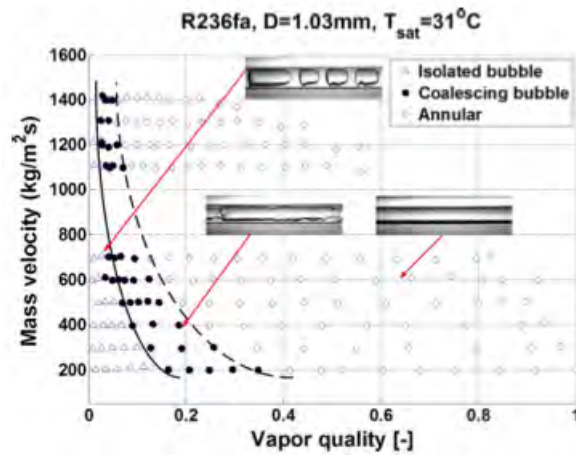

Figure 2: Flow pattern transition lines for R236fa. Extracted from Ong and Thome (2011).
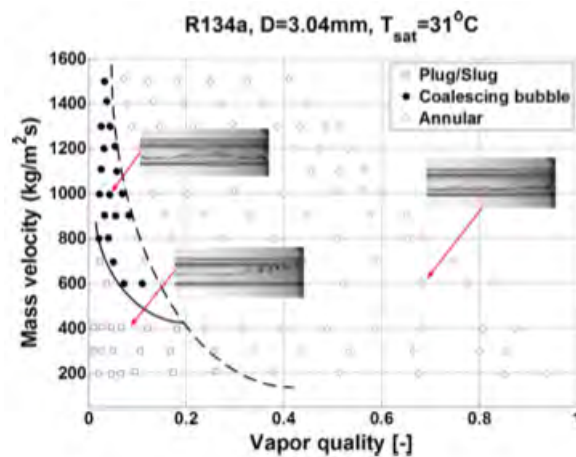

Figure 3: Flow pattern transition lines for R134a. Extracted from Ong and Thome (2011).

as an example. It is our interest in this work to propose an addition to the ALE/FE approach to be able to resolve computationally bubble coalescence phenomena. Certainly, one of its most powerful characteristics is treating both liquid and gas phases with the same computational mesh. This is a positive point as regards tracking the interfacial dynamics.

This paper is organized as follows: Section 2. introduces the equations governing the two-phase fluid flow system and explains the scheme used to calculate important properties such as curvature; Section 3.describes an algorithm based on ALE/FE coupled to LS approach to address the coalescence problem as well as the overall methodology. We consider a bidimensional simplified model of head-on coalescence between two circular bubbles with analogous extension to three-dimensional cases; in the Section 4.some numerical results are showed and followed by discussions, and Section 5.ends up with the conclusions.

2. GOVERNING EQUATIONS

The governing equations used in this work take an ALE frame into account in their formulation. Some arbitrariness is allowed to the mesh nodes movement when the ALE description is used. For instance, the nodes may either stay stationary as an Eulerian frame, move together with the fluid as in the Lagrangian frame, or even move in a specified direction. This freedom permits a continued rezoning capability. Additionally, larger distortions are handled with good resolution.

To reach its goal, the ALE methodology establishes an "intermediary" domain called the *referential domain* to make an interplay between the material and spacial domains used to map the movement. In mathematical language, the ALE description can be understood through homeomorphisms. According to Donea *et al.* (2004), from these mappings, the velocity field is called the *convective velocity* and can be written as

$$c = v - \hat{v}, \tag{3}$$

where v is the *fluid velocity* and $\hat{v}$ is the *mesh velocity*.

For the two-phase modeling discussed here, we consider that the fluid properties are respectively constant everywhere inside the liquid and vapor phases, differing by a discontinuity jump only over the interface locus. In other words, we use a separated flow model that leads to a simplified version of the momentum equation (see, for instance, Hewitt and Hall-Taylor (1970)). Furthermore, the incompressibility condition is assumed to be valid for both phases. Gravitational and interfacial forces are considered to be present in the model as well. These hypotheses lead to the following pair of adimensional equations valid for each phase separately.

$$\rho \left(\frac{\partial v}{\partial t} + c \cdot \nabla v \right) = -\nabla p + \frac{1}{Re} \nabla \cdot \left[\mu \left(\nabla v + \nabla v^T \right) \right] + \frac{\rho}{Fr^2} g + \frac{1}{We} f \tag{4}$$

$$\nabla \cdot v = 0, \tag{5}$$

where v is the fluid velocity, p the pressure, ρ the density, μ the dynamic viscosity, g the gravitational force, and t the adimensional time. Fr and We have already been defined in the Eq. (1), while f accounts for interfacial effects and is given by

$$f = \sigma \kappa n, \tag{6}$$

where σ is the surface tension, κ is the curvature locally evaluated over the interface, and n is the unit normal vector over each interface node pointing outward the vapor phase. The discrete process to calculate the unit normal vector in two-dimensional domains takes two properties into account. Firstly, the interface is a closed curve represented by a set of linear elements and, hence, structured. That is to say, each interface node has always two neighbor elements. Secondly, the normal vectors for each neighbor element can be obtained by orthogonalizing the unit tangent vectors to each element, which, in fact, are obtained by normalizing the element length itself. In turn, the normal vector for the shared node is evaluated by summing the contributions of the normal elemental vectors. This scheme is depicted in the Fig. 4. Mathematically, if $n(e_{L,i}), n(e_{R,i})$ are the unit normal vectors evaluated over the neighbor elements respectively at left and at right of the interface node x_i, then,

$$n(e_{L,i}) = R_{\pi/2} \left[t(e_{L,i}) \right], \quad n(e_{R,i}) = R_{\pi/2} \left[t(e_{R,i}) \right], \tag{7}$$

where

$$t(e_{L,i}) = \frac{x_{L,i} - x_i}{||x_{L,i} - x_i||}, \quad t(e_{R,i}) = \frac{x_{R,i} - x_i}{||x_{R,i} - x_i||}. \tag{8}$$

Above, $x_{L,i}, x_{R,i}$ are the vertices of the neighbor elements not matching the interface node and $t(e_{L,i}), t(e_{R,i})$ their respective unit tangent vectors generated by the rotation matrix $R_{\pi/2}$. Directly from Eqs. 7 and 8, we get

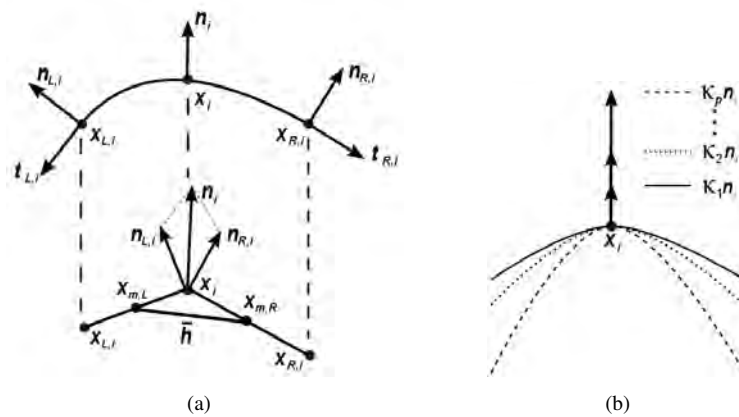$$n(x_i) = n(e_{L,i}) + n(e_{R,i}) = R_{\pi/2} \left[t(e_{L,i}) + t(e_{R,i}) \right]. \tag{9}$$

Figure 4: Scheme for the calculation of the curvature: (a) continuous and discrete versions; (b) effect of the curvature upon the normal vector at $\boldsymbol{x}_i$.

Meanwhile, the curvature $\kappa(\boldsymbol{x}_i)$ is evaluated for each interface node by an approximation adapted from a formulae set of the Frenet's frame, or, even more formally, *Frenet-Serret Theorem* - see Bloch (1956) - for curvature and torsion. Equation 10 is the continuous version of one among the Frenet's formulae relating κ and the unit vector tangent $\boldsymbol{t}$ to the interface.

$$\kappa \boldsymbol{n} = \frac{\partial \boldsymbol{t}}{\partial s} \approx \frac{\boldsymbol{t}(e_{L,i}) - \boldsymbol{t}(e_{R,i})}{\bar{h}}. \tag{10}$$

Since the elements $e_{L,i}, e_{R,i}$ do not necessarily have the same size, the evaluation of $\kappa(\boldsymbol{x}_i)$ is undertaken as an average distribution over the mean length $\bar{h}$ of the neighbor elements given by

$$\bar{h} = \frac{1}{2}(h_L + h_R), \tag{11}$$

where h_L, h_R are the lengths of the neighbor elements. Also depicted in Fig. 4, at left, it is seen that $\bar{h}$ binds the two centroidal points $\boldsymbol{x}_{m,L}, \boldsymbol{x}_{m,R}$. At right, a sketch was added only to illustrate how κ affects the normal vector $\boldsymbol{n}_i$ by stretching it. From Eq. 10, we infer that the higher the tangential derivative along the interface, the higher the norm of the vector $\kappa \boldsymbol{n}_i$, because if, for instance, we choose a sequence (κ_p) such that $\kappa_1 < \kappa_2 < \ldots < \kappa_p$, then

$$||\kappa_1 \boldsymbol{n}_i|| < ||\kappa_2 \boldsymbol{n}_i|| < \ldots < ||\kappa_p \boldsymbol{n}_i||. \tag{12}$$

In other words, high curvatures tend to magnify the normal vector at $\boldsymbol{x}_i$.

Additionally, the Heaviside function is used in this work to manage points near to interface sites. It identifies if an arbitrary node belongs to the liquid phase, the vapor phase, or the interface. Since its image is, in fact, the discrete set $\{0, 1\}$, it is not unexpected to assign a mean value to identify interface nodes and define H as

$$H(\boldsymbol{x}) := \begin{cases} 0, & \text{if } \boldsymbol{x} \equiv \boldsymbol{x}_L \\ 0.5, & \text{if } \boldsymbol{x} \equiv \boldsymbol{x}_I \\ 1, & \text{if } \boldsymbol{x} \equiv \boldsymbol{x}_V, \end{cases} \tag{13}$$

where the subscripts L, I, V stands for liquid, interface, and vapor.

Equation 6 is a version of the Continuum Surface Force (CSF) model introduced by Brackbill *et al.* (1992), in which the surface force was redesigned as a volumetric force. In terms of the aforementioned equations, the force $\boldsymbol{f}$ in the Eq. (6) is obtained by a FE procedure that solves the linear system given by

$$\boldsymbol{M}\boldsymbol{f} = \boldsymbol{\Sigma}\boldsymbol{G}H, \tag{14}$$

where $\boldsymbol{\Sigma}$ is a diagonal matrix whose entries are given by $\sigma\kappa_1, \sigma\kappa_2, \ldots, \sigma\kappa_P$, for P pressure nodes over the mesh. $\boldsymbol{G}$ is the gradient discrete matrix and H the Heaviside function.

3. METHODOLOGY: ALE/FE AND LEVEL-SET FOR BUBBLE COALESCENCE MODELING

In this section, we explain a combined methodology to simulate coalescing bubbles. On the one hand, the ALE/FE approach provides the main capability to remesh the thin film local region reconnecting computational elements affected by topological change. On the other hand, the LS strategy is focused on summing a function whose support is liable to

determine the coalescing region. For simplicity, we start from an idealized two-dimensional model describing a "head-on" coalescence process between two rounded bubbles immersed in a liquid. Even though this model does not take the deformation of the bubbles' surfaces into account, the idea behind it can be conveniently conveyed to three-dimensional problems with different bubble shapes because it is focused on the thin liquid film region and not strictly on any transient topology experienced by the surfaces.

First of all, it is convenient to use some definitions. Let $\Omega_{b,1}$ ($\Gamma_{b,1}$) and $\Omega_{b,2}$ ($\Gamma_{b,2}$) be the domains (boundaries) of the bubbles in vapor phase, and $\Omega_{f,\epsilon}$ the in-between region of the liquid thin film near the bubbles. ϵ is a small parameter related to the minimum distance between $\Gamma_{b,1}$ and $\Gamma_{b,2}$. In this discussion, the bulk region of liquid far from the thin film region whose scale is much bigger than ϵ is left untreated. It is feasible to set extreme points ($\bar{x}_1, \bar{x}_2$, where $\bar{x}_1 \in \Gamma_{b,1}$ and $\bar{x}_2 \in \Gamma_{b,2}$) to set limits for the minimum distance between the bubbles. Figure 5 depicts the idealized two-dimensional model, whereas Fig. 6 is an augmented view of the continuous thin film region.
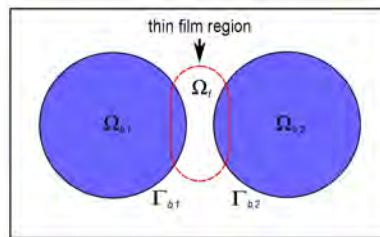

Figure 5: Two-dimensional idealized model for two near bubbles instantly before head-on coalescence.
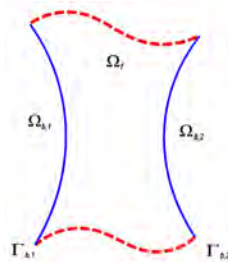

Figure 6: Augmented view of the liquid thin film region between two near bubbles.

In order to represent discretely the coalescence process through the ALE/FE approach, we will refer to Fig. 7, which is a sequential sketch showing the coalescence in three steps. For now, it is enough to recognize the edges in black representing the part of the mesh defined as vapor phase; the edges in red, the liquid phase, and the edges in blue, the interfaces. As we have already noted at first glance, one of the main characteristics of the ALE/FE methodology is to describe the bubbles interfaces as nodes, edges, and faces. In this manner, the interfaces $\Gamma_{b,1}, \Gamma_{b,2}$ are made up by interconnected edges whose nodes are part of the same mesh used to discretize the liquid phase. For the sake of this sharing, the elements belonging to the thin film region can be tracked and identified as elements in coalescence so that they are, later, carried forward to the vapor phase and marked as elements of this phase.

With reference to the Fig. 7, the dashed green line represents the distance ϵ between the bubbles. In (a) the elements filled in red were intentionally marked as coalescing elements in this explanation. Since the elements are identified, geometrical operations (insertion, deletion, and flipping) are performed upon the nodes and edges in order to adapt the mesh, keep its quality and correct eventual mass unbalance. This step is represented in (b). The edges in yellow are inserted after the deletion operations that occurr to break up the interface and mediate the merging process. That is to say, the liquid is squeezed out while the thin film retracts and the onset of the coalescence starts off. In the sequel, (c) depicts the third step, when the coalescence process is evolving. At this stage, the yellow edges were replaced with black edges to highlight the merging process. As the simulation runs, similar transformations tend to be carried out by the code for the elements within the thin film region that obey the proximity criterion based on the minimum distance ϵ.

The minimum distance between the bubbles can be calculated by using the well-known $\mathbb{R}^n$ formula for distance between vectors

$$d(\boldsymbol{x}, \boldsymbol{y}) = \left[\sum_{i=1}^{n} (x_i - y_i)^2 \right]^{1/2} \tag{15}$$

if the arguments above are replaced with the extreme points $\bar{x}_1$ and $\bar{x}_2$. On the other hand, the minimum distance has to be determined by a numerical procedure which should span all the pairs of nodes belonging to $\Gamma_{b,1}$ and $\Gamma_{b,2}$, but inside a combination zone limited by another numerical artifice. Consequently, this combination zone tends to reduce calculations,
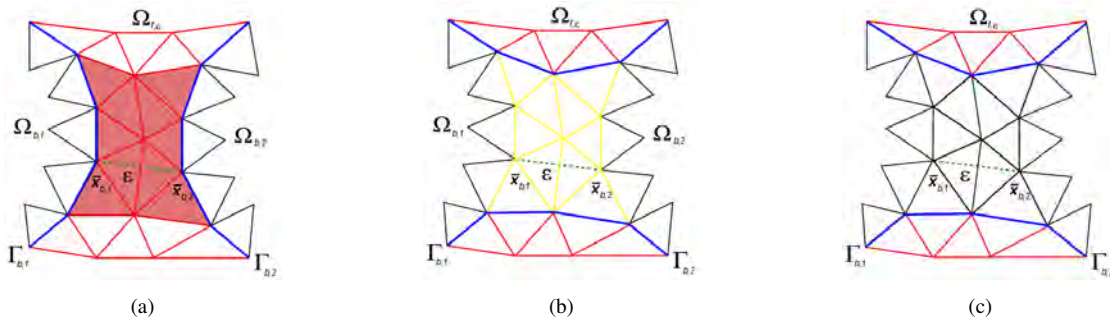
(a)   (b)   (c)

Figure 7: ALE/FE discretization of the thin film region between two bubbles: (a) before coalescence; (b) onset of coalescence; (c) during coalescence.

since it is not necessary to go through all the interface nodes in order to find the minimum distance. In Quan *et al.* (2009), an algorithm based on the creation of a combination zone to simulate the head-on bubble coalescence is tested. However, the author points out that not only the combination zone but also the process to determine it is a task depending on the problem and should be tuned for each case.

In seeking to determine the combination zone between the two bubbles, we invoke here a LS context by defining particular functions. These functions, on the whole, not only specify the interface nodes, but also manage the local smoothing of the coalescing elements. Let ϕ be the standard level-set function defined as

$$\phi(\boldsymbol{x}) := \min_{\boldsymbol{x}_{I,k} \in \Gamma_{b,k}} \{ d(\boldsymbol{x}, \boldsymbol{x}_{I,1}), d(\boldsymbol{x}, \boldsymbol{x}_{I,2}) \} . \tag{16}$$

Since two interfaces are nearby each other, ϕ is introduced to detect the interface nodes belonging to the boundary of the bubbles and responding for the curve of contour zero. Before the coalescence, the bubbles are separated by a tiny distance. However, numerically, it is convenient to establish ϵ as the limiting parameter from which the coalescence should start off. Consequently, all the elements inside this delimited area will undergo geometrical transformations and will be pending for remeshing. In the new methodology now introduced, we wish that the coalescing elements are kept subordinate to a function W_ϵ whose support will affect directly the zero contour of the level-set function. In other words, W_ϵ pervades the combination zone to cause smoothness in the curve identified by $\phi(\boldsymbol{x}) = 0$. We call W_ϵ a *blending function*, which is defined as

$$W_\epsilon(\boldsymbol{x}) := \begin{cases} 1 - \dfrac{\|\boldsymbol{x}\|}{\epsilon}, & \text{if } \boldsymbol{x} \in \Omega_{f,\epsilon} \\ \\ 0, & \text{otherwise.} \end{cases} \tag{17}$$

Similarly to ϕ, W_ϵ also is cone-shaped, but centered in the combination zone and having a small support. When W_ϵ "pierces" ϕ and blends their contributions, a new function $\tilde{\phi}$ is created by defining

$$\tilde{\phi}(\boldsymbol{x}) := \phi(\boldsymbol{x}) - 2\epsilon W_\epsilon(\boldsymbol{x}). \tag{18}$$

Further details about $\tilde{\phi}(\boldsymbol{x})$ are given in the next section.

4. NUMERICAL RESULTS AND DISCUSSIONS

Some numerical tests are shown in this section. Figure 8 is a plot of $\tilde{\phi}$ for a two-dimensional domain of size $6D \times 4D$, where D is the diameter of the bubbles. The small coniform hill in the middle displays the contribution of W_ϵ. As a result, the contour zero of $\tilde{\phi}$ is a new curve intercepted by a central bulb-like neck which foreshadows a bridge for the coalescence. Figure 9 shows the shaded contour zero of $\tilde{\phi}$ as well as the resulting curve under a simple layout.

Additionally, we present a numerical simulation of a oscillating drop immersed in a stagnant liquid in order to show the capability of the ALE/FE method to capture topological changes of surface. This is a benchmark test concerning code validation and was performed by dos Anjos (2012) under a three-dimensional version. The domain of simulation is a square with dimensions $8D \times 8D$, where D is the drop diameter. Initially, the drop is slightly symmetrically ellipsoidal in relation to the $x-$axis. Apart from gravity effects, the drop is weakly perturbed, so oscillating with an induced frequency ω of

$$\omega = \left[\frac{(n^3 - n)\sigma}{(\rho_{in} + \rho_{out})r^3} \right]^{1/2} \tag{19}$$
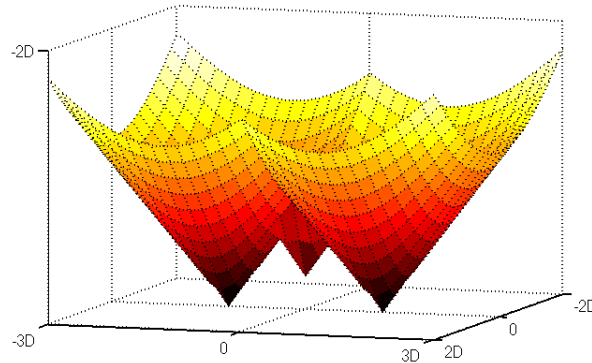
Figure 8: Function $\tilde{\phi}$ plotted over the coalescence domain $6D \times 4D$.

(a)   (b)
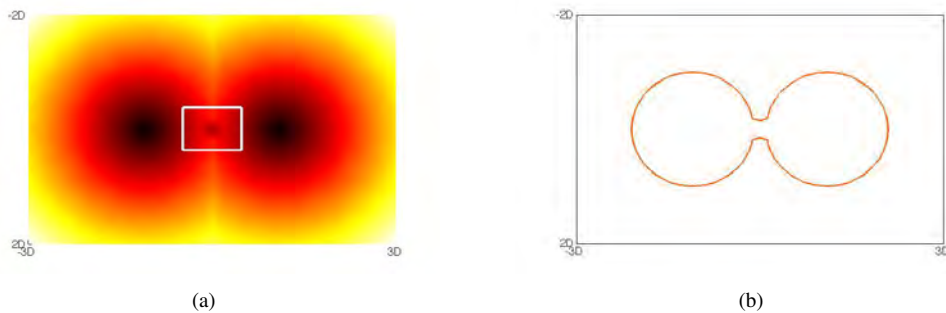
Figure 9: Contour zero of $\tilde{\phi}$: (a) shaded, with the white rectangle highlighting the coalescing bridge; (b) simple curve.

and decay amplitude of

$$a(t) = a_0 e^{-t/\tau}. \tag{20}$$

In the Eqs. 19 and 20, n is the mode of perturbation, σ is the surface tension coefficient, ρ_{in}, ρ_{out} the densities of the internal and external fluids, r the drop radius, and ν the kinematic viscosity. When varying its diameter, the drop surface obeys the following time-depending equation

$$y(t) = y_0 + a(t)cos(\omega t), \tag{21}$$

where y_0 is the $y-$axis initial coordinate.

For the present simulation, all the parameters before mentioned were set as $n = 2$, $\sigma = 1$, $\rho_{in} = 1$, $\rho_{out} = 0.001$, $r = 0.5$, $\nu = 1$, $a_0 = 0.1r$, and $y_0 = 0$. Given the small external viscosity imposed, the oscillatory process is governed by interfacial forces and counterbalanced by convective forces. In the Fig. 10, the image of the Heaviside function is depicted for the oscillating drop both in overview and augmented views. As can be seen, the interface region is notably distinguished by colors and higher refinement.

(a)   (b)
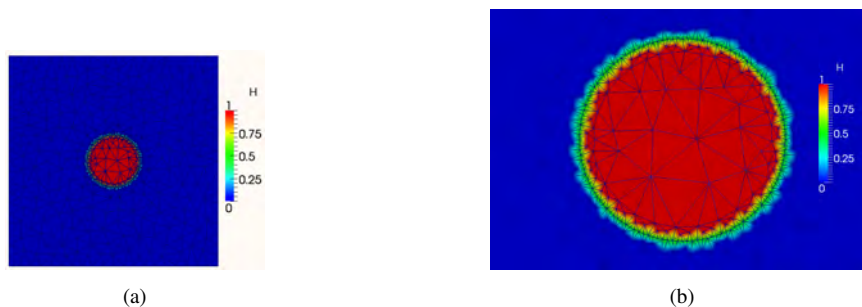
Figure 10: Heaviside function detecting the interface region as well as the liquid and vapor phases for the oscillating drop test: (a) overview of the two-dimensional FE mesh; (b) FE mesh zoomed in.

Five levels of adaptive refinement were applied over the interface mesh as exhibiting the accuracy of the method to accompany the topological changes of the interface. Figure 11 is a plot of the variation of amplitude *versus* time of the
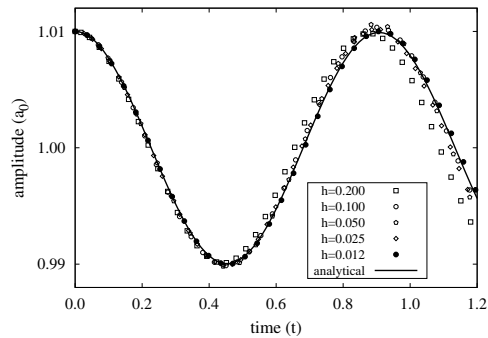
Figure 11: Comparative plot of the analytical diameter $y-$variation for the oscillating drop test against five increasing levels of interface local refinement.

drop, i.e., it shows how the $y-$diameter oscillates along the time. Between the coarsest mesh, whose elements have a characteristic length of $h = 0.2$, and the finest mesh, with $h = 0.012$, three intermediary levels were simulated: $h = 0.1$, $h = 0.05$, and $h = 0.025$. Overall, the numerical solutions tend to the analytical solution and, consequently, better accuracy is achieved as the mesh is refined. Three particular plots of the mesh velocity field were extracted from the time
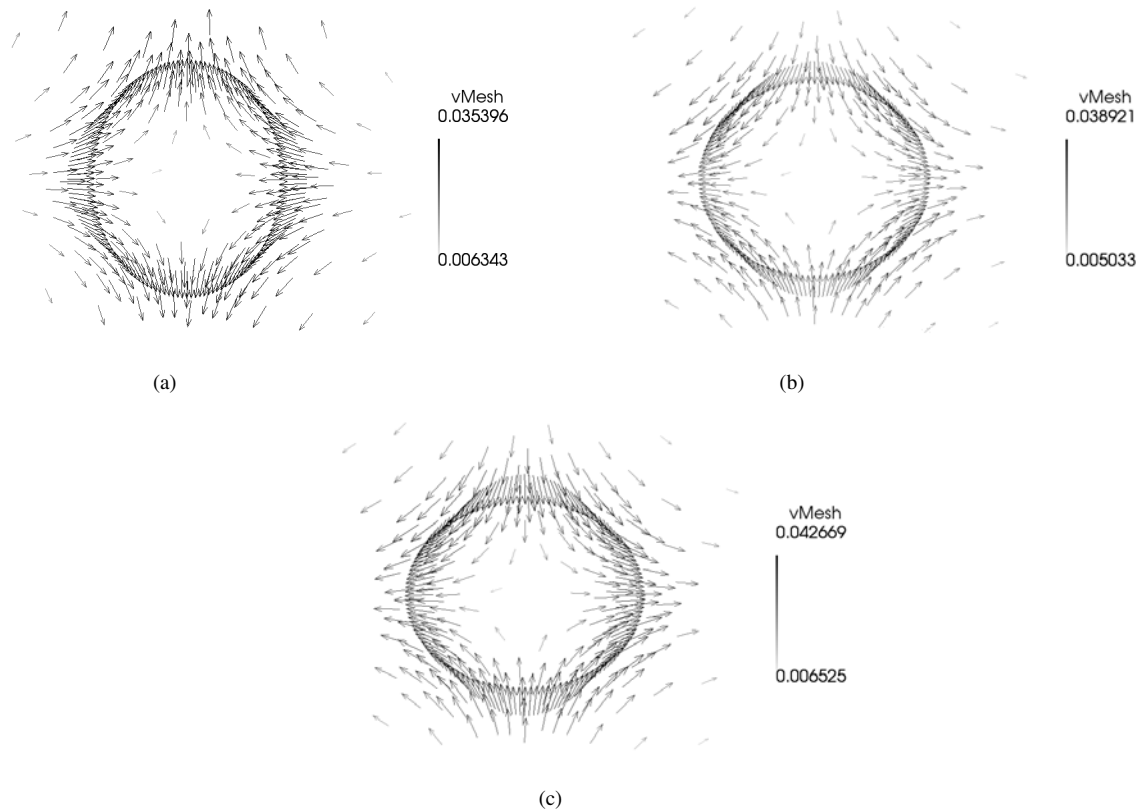

Figure 12: Mesh velocity field surrounding the oscillating drop for three different times: (a) $t \approx 0.20$; (b) $t \approx 0.59$; (c) $t \approx 0.71$.

interval $T = [0, 1.2]$ for a simulation with level $h = 0.025$, $CFL = 0.8$ and convenient time instants chosen inside T, namely, $t \approx 0.20$; $t \approx 0.59$, and $t \approx 0.71$ are shown in the Fig. 12. Inside T, the drop completes a period of oscillation and the mesh velocity field changes accordingly as it can be observed. In (a), the drop begins to dilatate along the $y-$axis because of the perturbation imposed. Simultaneously, both the mesh points of the interface and those surrounding it are moved in order to follow the topological change of the surface and the external fluid layers pushed out. Inasmuch as the incompressibility constraint must to be satisfied, the drop is flattened in the $x-$axis. In (b), the drop is going the inverse process and dilatates along the $x-$axis until achieving the sequential shape depicted in (c) after a few seconds. This process is repetitive along the periods of oscillation, other than by the direction of the vectors that is inverted after each

peak of amplitude and does not require extensive analysis. Moreover, very small velocities are, indeed, expected to occur for the drop as it can be verified in each plot, where the magnitude of the mesh velocity field is scaled by the size of the vectors.
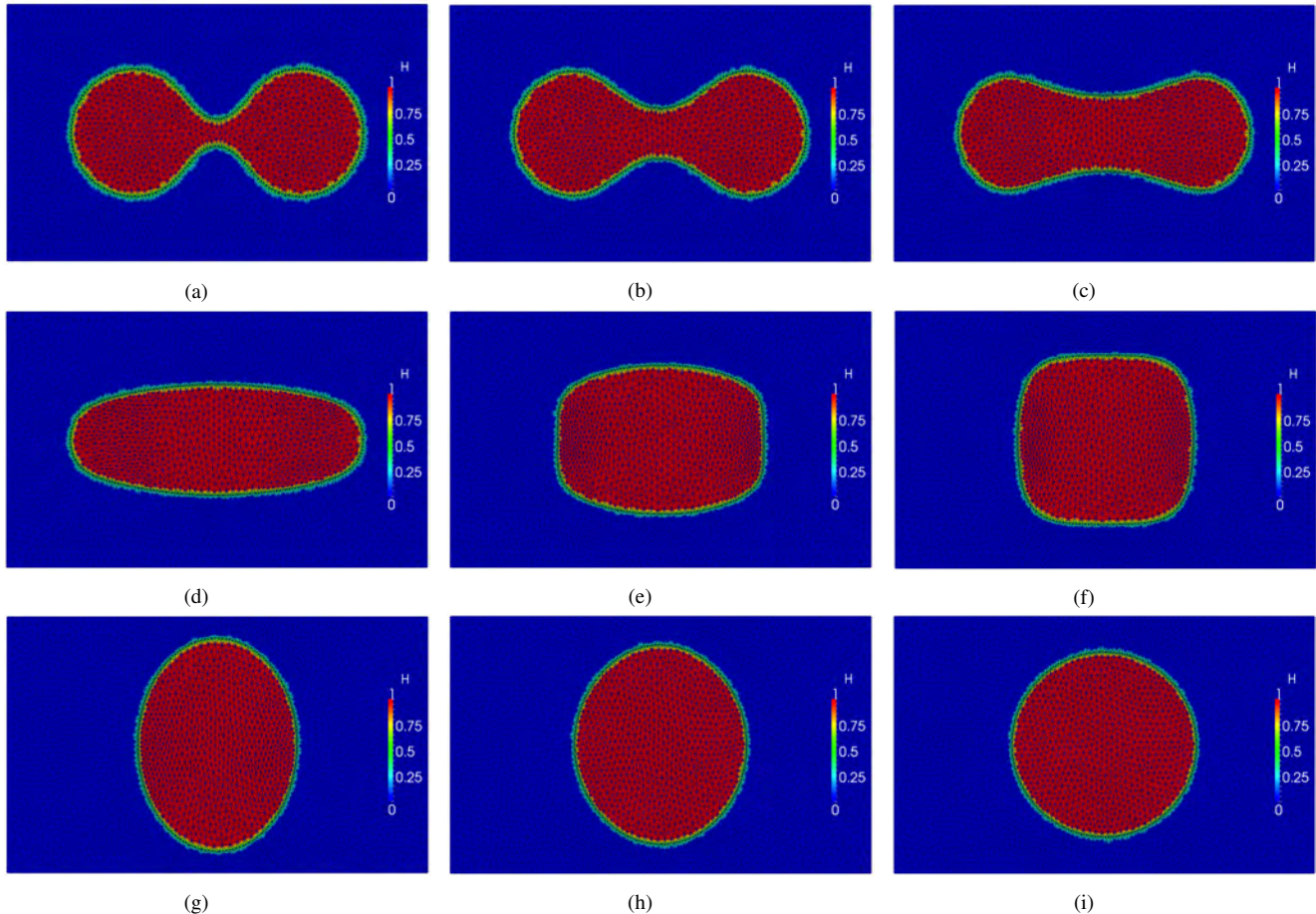

Figure 13: Simulation of the coalescing bubbles: (a) $t \approx 0.17$; (b) $t \approx 0.33$; (c) $t \approx 0.52$; (d) $t \approx 0.85$; (e) $t \approx 1.48$; (f) $t \approx 1.94$; (g) $t \approx 3.08$; (h) $t \approx 4.46$, and (i) $t \approx 5.49$.

In order to verify that the ALE/FE code is capable to simulate the topological changes following the coalescence between the two bubbles, the Fig. 13 shows a series of pictures extracted along the evolution of the bubbles already coalesced. For better recognition of the phases and interface, plots of the Heaviside function are used again. In this simulation, both the governing parameters and imposed conditions are similar to the oscillating drop test, except for the CFL number (now unitary) and slight changes in the mesh refinement control.

The simulation starts off from the configuration described in the Fig. 9. As the step times advance, the central bulb is enlarged vertically, so bridging the coalescence as depicted in (a), (b), and (c). Since the surface tension works to minimize the surface area, the curvature at the upper and lower regions of the bulb is reduced and the two bubbles begin to seem a unique bubble, which achieves a sudden ellipsoidal shape followed by horizontal shrinking. This is depcited in (d), (e). and (f). In the last row of snapshots, (g), (h), and (i), the bubble undergoes a dumping effect that begins from the highest vertical stretching unto recovering a circular shape. Posteriorly, the bubble attains a behaviour slightly oscillatory due to the remaining effect of dumping, but theses steps were omitted.

5. SUMMARY AND CONCLUSIONS

Purposes of this paper were: to address the process of bubble coalescence in two-phase flows with focus here on a coupled approach between the ALE/FE and LS methodologies; to propose a numerical strategy to model the coalescence of two spherical bubbles by delimiting a combination zone that confines the liquid thin film region near the bubbles, and to present inceptive numerical results guided by the presented idea.

The standard level-set function was enhanced by a new blending function whose support determines locally the coalescing zone. Cumulatively, this cone-shaped function produces a smoothing effect upon the original level-set function which reflects over the curve of contour zero when forming a central bulb that induces the coalescence. Thereafter, the instantaneity of the real coalescence is condensated into a numerical step.

Additionally, a benchmark test based on the oscillation of a drop immersed in a stagnant liquid was performed in order to assure that the ALE/FE code is able to deal with calculations of surface tension in a reasonably precise way. The results showed good convergence in comparison with the analytic solution. Similarly, the test of the bubbles already coalesced was appended to show the capabilites of the code to evaluate fairly the topological changes arising from the simple collision between two circular bubbles.

Although exist several experimental studies that firm the important role played by the coalescing phenomena in two-phase flows, mainly around transition regimes, this issue still is challenging for MCFD methods and numerics, inasmuch as interfacial effects are difficult to capture but they dominate the liquid thin film region. On the other hand, the introductory numerical results obtained here underpin the quality of ALE/FE to discretize profitably the interface of an arbitrary bubble immersed in a liquid solution and led us to the pursuit of deeper investigations that include LS schemes for applications enfolding bubble coalescence. In this trail, this numerical model also seeks precise concordance with experimental data and observation. Advancements and improvements in the root idea of the method were presented and the main research targets to remaining study include: extension to three-dimensional cases and modeling of the coalescence between bubbles with arbitrary surface topology, such as Taylor bubbles evolving in microchannels.

6. ACKNOWLEDGEMENTS

7. REFERENCES

Agrawal, K., 2013. "Bubble dynamics and interface phenomenon". *Journal of Engineering and Technology Research*, Vol. 5, No. 3, pp. 42–50.

Bloch, E.D., 1956. *A First Course in Geometric Topology and Differential Geometry*. Birkhauser.

Brackbill, J., Kothe, D.B. and Zemach, C., 1992. "A continuum method for modeling surface tension". *Journal of computational physics*, Vol. 100, No. 2, pp. 335–354.

Cheng, L., Ribatski, G. and Thome, J., 2008. "Two-phase flow patterns and flow-pattern maps: fundamentals and applications". *Applied Mechanics Reviews*, Vol. 61, No. 5, p. 050802.

Clift, R., Grace, J. and Weber, M.E., 1978. *Bubbles, Drops and Particles*. Academic Press.

Consolini, L. and Thome, J., 2010. "A heat transfer model for evaporation of coalescing bubbles in micro-channel flow". *International Journal of Heat and Fluid Flow*, Vol. 31, No. 1, pp. 115–125.

Coulibaly, A., Lin, X., Bi, J. and Christopher, D.M., 2013. "Bubble coalescence at constant wall temperatures during subcooled nucleate pool boiling". *Experimental Thermal and Fluid Science*, Vol. 44.

Donea, J., Huerta, A., Ponthot, J.P. and Rodríguez-Ferran, A., 2004. "Arbitrary lagrangian–eulerian methods". *Encyclopedia of computational mechanics*.

dos Anjos, G.R., 2012. *A 3D ALE Finite Element Method for Two-Phase Flows with Phase Change*. Ph.D. thesis, EPFL - École Polytechnique Fédéral de Lausanne, Switzerland.

Ekambara, K., Sanders, R.S., Nandakumar, K. and Masliyah, J., 2012. "Cfd modeling of gas-liquid bubbly flow in horizontal pipes: Influence of bubble coalescence and breakup". *International Journal of Chemical Engineering*, Vol. 2012.

Groß, S., Reichelt, V. and Reusken, A., 2006. "A finite element based level set method for two-phase incompressible flows". *Computing and Visualization in Science*, Vol. 9, No. 4, pp. 239–257.

Hewitt, G.F. and Hall-Taylor, N., 1970. *Annular Two-Phase Flow*. Pergamon Press.

Jingliang, B., Xipeng, L. and Christopher, D.M., 2012. "Effects of bubble coalescence dynamics on heat flux distributions under bubbles". *AIChE Journal*, Vol. 59, No. 5, pp. 1735–1745.

Julia, J.E. and Hibiki, T., 2011. "Flow regime transition criteria for two-phase flow in a vertical annulus". *International Journal of Heat and Fluid Flow*, Vol. 32, No. 5, pp. 993–1004.

Li, B. and Shoppie, J., 2011. "An interface-fitted finite element level set method with application to solidification and solvation". *Communications in Computational Physics*, Vol. 10, No. 1, p. 32.

Michaelides, E.E., 2006. *Particles, Bubbles and Drops: Their Motion, Heat and Mass Transfer*. World Scientific.

Mier-Torrecilla, M.d., Idelsohn, S. and Oñate, E., 2011. "Advances in the simulation of multi-fluid flows with the particle finite element method. application to bubble dynamics". *International Journal for Numerical Methods in Fluids*, Vol. 67, No. 11, pp. 1516–1539.

Ong, C. and Thome, J., 2011. "Macro-to-microchannel transition in two-phase flow: Part 1–two-phase flow patterns and film thickness measurements". *Experimental Thermal and Fluid Science*, Vol. 35, No. 1, pp. 37–47.

Osher, S. and Fedkiw, R.P., 2001. "Level set methods: an overview and some recent results". *Journal of Computational physics*, Vol. 169, No. 2, pp. 463–502.

Quan, S., 2011. "Simulations of multiphase flows with multiple length scales using moving mesh interface tracking with adaptive meshing". *Journal of Computational Physics*, Vol. 230, No. 13, pp. 5430–5448.

Quan, S., Lou, J. and Schmidt, D.P., 2009. "Modeling merging and breakup in the moving mesh interface tracking method for multiphase flow simulations". *Journal of Computational Physics*, Vol. 228, No. 7, pp. 2660–2675.

Quan, S. and Schmidt, D.P., 2007. "A moving mesh interface tracking method for 3d incompressible two-phase flows". *Journal of Computational Physics*, Vol. 221, No. 2, pp. 761–780.

Revellin, R., Agostini, B. and Thome, J.R., 2008. "Elongated bubbles in microchannels. part ii: Experimental study and modeling of bubble collisions". *International Journal of Multiphase Flow*, Vol. 34, No. 6, pp. 602–613.

Shen, X., Hibiki, T., Ono, T., Sato, K. and Mishima, K., 2012. "One-dimensional interfacial area transport of vertical upward bubbly flow in narrow rectangular channel". *International Journal of Heat and Fluid Flow*, Vol. 36, pp. 72–82.

Sousa, F. and Mangiavacchi, N., 2005. "A lagrangian level-set approach for the simulation of incompressible two-fluid flows". *International journal for numerical methods in fluids*, Vol. 47, No. 10-11, pp. 1393–1401.

8. RESPONSIBILITY NOTICE

The authors are the only responsible for the printed material included in this paper.